Metabolomic Changes in the Rat Retina After Optic Nerve Crush

Marta Agudo-Barriuso,[1,2] Agustín Lahoz,[3] Francisco M. Nadal-Nicolás,[1,2] Paloma Sobrado-Calvo,[2] Marina Piquer-Gil,[4] Manuel Díaz-Llopis,[5] Manuel Vidal-Sanz,[2] and José L. Mullor[4,6]

[1]Unidad de Investigación, Hospital Clínico Universitario Virgen de la Arrixaca, Fundación para la Formación e Investigación Sanitarias de la Región de Murcia, Instituto Murciano de Investigacón Biosanitaria, Murcia, Spain
[2]Departamento de Oftalmología, Facultad de Medicina, Regional Campus of International Excellence "Campus Mare Nostrum," Universidad de Murcia, Instituto Murciano de Investigación Biosanitaria, Murcia, Spain
[3]Unidad de Hepatología Experimental, Instituto de Investigación Sanitaria-Fundación Hospital La Fe, Valencia, Spain
[4]Instituto de Investigación Sanitaria-Fundación Hospital La Fe, Valencia, Spain
[5]Servicio de Oftalmología, Hospital La Fe, Departamento de Oftalmología, Universidad de Valencia, Valencia, Spain
[6]Bionos, SL, Biopolo La Fe Hospital La Fe, Valencia, Spain

Correspondence: Marta Agudo-Barriuso, Departamento Oftalmología Experimental, Facultad de Medicina, Campus Espinardo, 30100 Murcia, Spain;
martabar@um.es.
José L. Mullor, Instituto de Investigación Sanitaria, Fundación Hospital La Fe, Av. Campanar 21, Valencia 46009, Spain;
jlmullor@iislafe.es,
jlmullor@bionos.es.

Submitted: December 7, 2012
Accepted: May 9, 2013

Citation: Agudo-Barriuso M, Lahoz A, Nadal-Nicolás FM, et al. Metabolomic changes in the rat retina after optic nerve crush. *Invest Ophthalmol Vis Sci*. 2013;54:4249–4259.
DOI:10.1167/iovs.12-11451

Purpose. To identify metabolic pathways and metabolites affected by optic nerve crush that can act as predictors of the disease or therapeutic targets.

Methods. The left optic nerve of adult rats was intraorbitally crushed and retinas were dissected 24 hours or 14 days after the lesion ($n = 10$ per group). Metabolic profiling analysis was carried out by Metabolon, Inc. A total of 195 metabolites were unambiguously detected. Data were normalized and the regulated metabolites were identified after comparing the different conditions. Metabolite concentration changes were analyzed using single and multivariate statistical analysis to detect discriminatory metabolites. Functional clustering and meta-analysis of the regulated metabolites was run through the Metacore platform.

Results. Comparison of 24 hours versus control, 14 days versus control samples, and 24 hours versus 14 days identified 9, 19, and 32 regulated metabolites, respectively. Single and multivariate analysis identified a total of 27 and 36 metabolites to discriminate between control and 14 days and between 24 hours and 14 days, respectively. Enrichment analysis showed alterations in the amino acid, carbohydrate, and lipid metabolism, which were further linked to translation, oxidative stress, energy (glucose and tricarboxylic acid cycle), and apoptosis through ceramide pathways.

Conclusions. Our analysis differentiates a set of metabolites that clearly discriminate control and early-injury samples from late-injury samples. These metabolites could have potential use as diagnostic molecules.

Keywords: amino acid metabolism, carbohydrate, oxidative stress, glutathione, translation, ceramide, axotomy, multivariate data analysis, central nervous system, trauma

In glaucoma, the second most common leading cause of blindness,[1] retinal ganglion cells (RGCs) and their axons progressively degenerate, causing increasing visual deficits. Although the reasons underlying RGC death in glaucoma are not known, two main insults are believed to be involved: a crush-like injury to the RGC axons at the optic nerve head and/or an ischemic episode to the retinal vasculature (reviewed in Refs. 2 and 3).

Complete intraorbital optic nerve crush (IONC) is a model of acute traumatic axonal injury to the central nervous system that causes extended RGC degeneration and apoptosis. Additionally, while not being an exact model of glaucoma, IONC injury shares some common mechanisms with this disease.[4] In our rat IONC model, the optic nerve (ON) is crushed for 10 seconds, resulting in complete interruption of the retinofugal projection, as demonstrated by their failure to transport tracers orthogradely and retrogradely.[5] IONC triggers a reproducible massive RGC degeneration, and by day 14 more than 80% of their population is lost.[5–7] In the early phase of degeneration, there is a diffuse loss of RGCs throughout the entire retina, which is significantly detected 3 days after the lesion.[6,7] At the molecular level, as early as 12 hours after the injury there are significant changes in the regulation of pro-death genes and proteins.[8,9] However, at 12 hours, anatomical RGC loss is not yet detected, suggesting that the commitment to death occurs earlier than previously anticipated. Furthermore, it is also observed that cellular metabolism itself is highly regulated by IONC.

Because of the different therapeutic implications for neuronal traumatic loss, many efforts have been devoted to investigate neuroprotective therapies to delay or stop axotomy-induced RGC death. Among these, neurotrophin delivery is one of the most successful.[5,10–17] However, the different therapies tested have been unsuccessful in permanently rescuing injured RGCs.

IONC regulates several apoptotic pathways in the retina[8,9] and, thus, neuroprotective therapies may have missed important target molecules or the correct time-window for action. In

addition, the complexity of signaling pathways involved in RGC degeneration makes it difficult to choose the correct target molecule. To successfully mitigate RGC loss, it would be helpful to understand the full genetic and metabolic changes occurring during RGC death. This information could provide important information about key regulators of this process that could be used as prognostic or therapeutic molecules.

The analysis of the concentrations of a large collection of metabolites present in a given tissue in a given developmental, physiological, or pathological state provides a measure of the metabolic state of the cells.[18] The main goal of metabolomic studies is the identification of metabolic markers[19] that may help to discriminate healthy versus pathological conditions, such as infection,[20,21] cancer, [22–24] and chronic,[25] cardiovascular,[25–28] or neurodegenerative diseases.[25,29–33] Identification of metabolites as biomarkers for neurological diseases has been carried out since the 1990s (reviewed in Ref. 34). Nowadays, the –omics technologies allow disclosing the global changes in metabolites, proteins, or transcripts occurring in pathological versus healthy samples. Furthermore, combination of different –omics approaches, such as transcriptomic or proteomics with metabolomic, serves to create a more comprehensive picture of the changes associated to diseases or unsalubrious conditions, to better understand and therefore to treat them, and to pinpoint putative biomarkers.[29,35–43]

Here we have analyzed the metabolomic changes induced in the retina at two time points after IONC, early after the lesion when pro-death signals are overexpressed but the anatomical loss of RGCs is not yet observed, and late after the lesion when the acute wave of RGC death has finished.

Materials and Methods

Ethics Statement: Animal Handling, Anesthesia, and Analgesia

Twenty-five Sprague-Dawley female rats (180–220 g body weight) were used in this work. Animals were obtained from the University of Murcia breeding colony. All experimental procedures were carried out in accordance with the "Principles of laboratory animal care" (National Institutes of Health publication No. 85–23, revised 1985), the Office for Protection from Research Risks Public Health Service Policy of the Human Care and the Use of Laboratory Animals (revised 1986) and the US Animal Welfare Act, as amended, our institutional guidelines, European Union regulations for the use of animals in research, and the ARVO Statement for the Use of Animals in Ophthalmic and Vision Research.

Animals Groups Subjected to Surgery

For anesthesia, a mixture of xylazine (10 mg/kg body weight, Rompun; Bayer, Kiel, Germany) and ketamine (60 mg/kg body weight, Ketolar; Pfizer, Alcobendas, Madrid, Spain) was used intraperitoneally (i.p.). After surgery, an ointment containing tobramicin (Tobrex; Alcon, S.A., Barcelona, Spain) was applied on the cornea to prevent its desiccation. Rats were given oral analgesia (Buprex, buprenorphine 0.3 mg/mL; Schering-Plough, Madrid, Spain) at 0.5 mg/kg (prepared in strawberry-flavored gelatin) the day of the surgery and during the next 3 days.

All animals were killed with an i.p. injection of an overdose of pentobarbital (Dolethal, Vetoquinol; Especialidades Veterinarias, S.A., Alcobendas, Madrid, Spain).

Animals were divided into a control group ($n = 5$, i.e., 10 retinas) that did not undergo any experimental manipulation and one experimental group that received a complete IONC ($n = 20$). Sterile precautions were maintained for all surgical procedures. The left ON was intraorbitally crushed according to procedures that are standard in our laboratory.[5–7,9,44] Briefly, the left ON was crushed for 10 seconds at 3 mm from the optic disc using watchmaker's forceps. Before and after the procedure, the eye fundus was observed through the operating microscope to assess the integrity of the retinal blood flow. IONC-injured animals were killed 24 hours ($n = 10$) or 14 days post-IONC ($n = 10$).

After euthanasia, retinas were fresh dissected and immediately frozen on dry ice and afterward stored at −70°C until further processing. In control untouched animals, both retinas were extracted, whereas in the IONC-injured animals only the left retina was used.

Metabolomic Analysis

Frozen samples were sent to Metabolon, Inc. (Durham, NC). After successful completion of the range-finding study, samples were extracted and prepared for analysis using Metabolon's standard solvent extraction method. The extracted samples were split into equal parts for analysis on the gas chromatography/mass spectrometry (GC/MS) and liquid chromatography/MS/MS (LC/MS/MS) platforms. Also, several technical replicate samples were created from a homogeneous pool containing a small amount of all study samples.

Instrument variability was determined by calculating the median relative standard deviation (RSD) for the internal standards that were added to each sample before injection into the mass spectrometers (RSD: 7%). Overall process variability was determined by calculating the median RSD for all endogenous metabolites (i.e., noninstrument standards), present in 100% of the samples, which are technical replicates of pooled client samples (RSD: 11%). Both RSD values meet Metabolon's acceptance criteria.

Data Extraction and Quality Assurance. The data extraction of the raw MS data files yielded information that could be loaded into a relational database and manipulated without resorting to BLOB manipulation. Peaks were identified using Metabolon's proprietary peak integration software, and component parts were stored in a separate and specifically designed complex data structure.

Compound Identification. Compounds were identified by comparison with library entries of purified standards or recurrent unknown entities. Identification of known chemical entities was based on comparison with metabolomic library entries of purified standards. This analysis identified 195 metabolites.

Normalization. For studies spanning multiple days, a data normalization step was performed to correct variation resulting from instrument interday tuning differences. Essentially, each compound was corrected in run-day blocks by registering the medians to equal one (1.00) and normalizing each data point proportionately. For studies that did not require more than 1 day of analysis, no normalization was necessary, other than for purposes of data visualization.

Statistical Calculation. Global biochemical profiles were compared across the sample groups Normalized data were compared as follows: 24 hours-IONC versus control, 14 days-IONC versus control and 14 days versus 24 hours-IONC. The first two comparisons would disclose those metabolites regulated at each specific time point after the lesion (early and late), while comparison of both experimental groups would reveal those metabolites that change their expression level as the response to the injury progresses. Statistical analyses were performed with the program "R" (http://cran.r-project.org/). Significance test was the Welch *t*-test and metabolites were considered statistically significant when $P <$

Investigative Ophthalmology & Visual Science

0.05 and approaching significance when the P value trend was $0.05 < P < 0.1$.

Multivariate Data Analysis

Normalized data were exported to Simca P + v.12 from Umetrics (Windsor, UK) to perform multivariate statistical data analysis. Datasets were log transformed, mean-cantered, and unit variance scaled in a columnwise manner before carrying out statistical analyses. Further details of sample acquisition and data preprocessing can be found in a previously published procedure.[45] A principal component analysis (PCA) was done to achieve the natural interrelationship (grouping, clustering, or outlier detection) among samples and quality controls. Supervised multivariate data analysis was performed by partial least-squares discriminant analysis (PLSDA). The whole objective was to model the relationship between X (the MS dataset) and Y (classes). The quality of the PLSDA models was conducted by the typical cross validation (CV) procedure by leaving one-seventh of samples out of each round. The cumulative values of total Y explained variance (R^2), and the Y predictable variation (Q^2) close to one indicated proper modeling. To further assess model consistency and performance, a response permutation test ($n = 200$) was applied. In brief, permutation testing compares the original model's goodness of fit with the values obtained after class randomization.[46] All the classical statistical calculations were performed using the statistics software "R" (http://cran.r-project.org/).

In Silico Pathway Analysis

Functional clustering, enrichment, and pathway analysis of the regulated metabolites was carried out using Metacore (Thomson Reuters, New York, NY; http://www.genego.com/metacore.php) platform. Through this platform, metabolites were analyzed using the map folders, pathway maps, process networks, and metabolic networks enrichment analysis. Enrichment in Metacore metabolic or process networks and pathway maps is a step ahead of gene ontology clustering, as the networks and maps are built considering interactions between the objects (proteins/genes/metabolites).

Metacore maps represent a set of consecutive signals, or metabolic transformations, confirmed as a whole by experimental data or by inferred relationships. Thus, these are graphic images that reflect the consensus knowledge on specific functional components in the intracellular cell signaling, regulatory processes, metabolic processes, or disease-related processes. Maps are assembled into map folders divided onto regulatory, metabolic, disease, toxicity, and drug action sections, and thus form an ontology of their own kind.

The difference between the networks and the maps is that maps show canonical pathways in which the interaction information is well-published, meaning there are usually multiple references for each interaction, whereas the networks contain many interactions that have only a single article reference.

Statistical relevance of the found ontology matches is calculated as P value, or a probability of a match to occur by chance, given the size of the database. The lower the P value, the higher is the "nonrandomness" of finding the intersection between the dataset and the particular ontology. That, in turn, translates into a higher rating for the term matched. In particular, the more genes/proteins belong to a process/pathway, the lower the P value. Only those networks/maps that were statistically regulated ($P < 0.05$) at least at one time point were chosen.

Finally, we constructed custom signaling maps using curated interactions between objects (proteins and/or metabolites). To do this, proteins and metabolites of a given process or pathway were loaded into Metacore to generate networks. Networks were merged and subsequently depurated of nonregulated or side objects. Final networks were transferred to the Pathway Map Creator tool (Thomson Reuters) to create more visually friendly signaling maps.

Results

Metabolomic Analysis

Comparison between 24 hours post-IONC versus control samples identified nine metabolites with significant ($P < 0.01$) concentration changes; however, such a small group (nine metabolites) can also be detected by random chance. Comparison between the 14-day time point and the control identified 19 metabolites with significantly altered concentration levels. Finally, 32 metabolite levels were found to change when comparing both groups (Table 1). Additional metabolites showed significant concentration level changes; however, these differences were significantly skewed by outlier points in the data (Table 1). Affected metabolites were clustered in super- and subpathways. It is worth noting that most of these metabolites are lipids and amino acids. A more detailed enrichment analysis is shown below.

Most changes in concentration levels were observed at 14 days. Therefore, our biochemical interpretation below is based primarily on the comparison between control and the 14-day time point.

Multivariate Analysis

The MS data set containing the metabolic profile of each sample was exported to SIMCA-P for multivariate data analysis. First, a PCA analysis for sample clustering and outlier detection was performed. The PCA scores plot revealed that two data points belonging to the IONC-24 hours and IONC-14 days groups were severe outliers and were excluded from further chemometric analysis (Supplementary Fig. S1A). PCA analysis showed two clear clusters: 24 hours post-IONC and the control groups and 14 days post-IONC group (Supplementary Fig. S1B). Based on these results, further chemometric analysis focused on finding the metabolic signature responsible for separation between these two groups (i.e., control versus 14 days and 24 hours versus 14 days) were performed by PLSDA. Two PLSDA models were calculated after performing a variable importance in the projection (VIP) selection procedure.[45] Model validation was performed by typical 7-fold CV, the R^2 values indicated the goodness of the model and the Q^2 values estimated the model's predictive ability. These values were used to assess the performance of the model and to select the optimal number of principal components (t). The results suggested an optimal model performance. The models were further validated by a random class permutation test ($n = 250$). The R^2 and Q^2 intercepts of the validation plots were examined to confirm model validation. All the permutation models showed lower R^2 values when compared with the original R^2 value (i.e., real class). Furthermore, all Q^2 regression lines showed negative intercepts. These results strongly confirmed the validity of our models. The first two-component score plot of the PLSDA metabolites from control versus 24 hours post-IONC and 24 hours post-IONC versus 14 days post-IONC showed a complete class separation (Figs. 1A–D). Classes were clearly discriminated by the first component (t1) in both models. This result suggests that differences among samples

Investigative Ophthalmology & Visual Science

Table 1. Clustering and Fold Change of Statistically Regulated Metabolites

Super Pathway	Sub Pathway	Biochemical Name	Fold Change			VIP Score	
			24 h vs. Ctrl	14 d vs. Ctrl	14 d vs. 24 h	14 d vs. Ctrl	14 d vs. 24 h
Amino acid	Glycine, serine, and threonine metabolism	Betaine	1.17				
	Alanine and aspartate metabolism	Alanine*			0.81		2.03
		Aspartate		1.52		2.01	
	Lysine metabolism	Glutaroyl carnitine		0.46	0.57	2.64	2.20
		Pipecolate			*0.79*		1.89
	Phenylalanine and tyrosine metabolism	Tyrosine			1.40		2.06
	Tryptophan metabolism	C-glycosyltryptophan*			1.31		
	Glutamate metabolism	*Glutamate*			*0.96*		1.89
	Valine, leucine and isoleucine metabolism	Isovalerylcarnitine		1.71	1.53	2.20	2.12
	Cysteine, methionine, SAM, taurine metabolism	Cysteine*		1.78		1.98	
		Hypotaurine		1.70	1.97	1.995	2.13
		N-acetylmethionine		4.78	4.19	2.20	2.11
	Urea cycle; arginine-, proline-, metabolism	Arginine		1.12			
		Urea		1.46	1.36	2.34	2.26
		Proline	1.40				1.96
		N-acetylornithine*		0.75		2.21	2.03
	Polyamine metabolism	Putrescine*			1.65		2.05
	Guanidino and acetamido metabolism	4-guanidinobutanoate			0.71		2.04
	Glutathione metabolism	5-oxoproline			1.36		
		Glutathione, reduced (GSH)†		1.31	1.51		
		Glutathione, oxidized (GSSG)†		1.31	1.56		
		Ophthalmate		*0.87*			2.13
Peptide	Dipeptide	Leucylleucine*	0.68				
		Pro-hydroxy-pro*			0.49		2.10
	Dipeptide derivative	Anserine*		0.66		1.98	
		Carnosine		*0.7*			1.93
	Gamma-glutamyl	Gamma-glutamylglutamate*			1.27		
		Gamma-glutamylglutamine	0.80		1.43	1.95	2.37
Carbohydrate	Fructose, mannose, galactose, starch, and sucrose metabolism	Fructose		1.88	2.11	2.21	2.39
		Maltose	2.55	1.66		2.11	
		Sorbitol		1.64	1.67	2.04	2.0
	Glycolysis, gluconeogenesis, pyruvate metabolism	1,5-anhydroglucitol (1,5-AG)			1.23		2.12
		Glucose-6-phosphate (G6P)		2.75		1.99	
		Glucose		3.29	2.23	2.16	2.13
	Amino sugars metabolism	*Erythronate*			*0.94*		1.97
Energy	Krebs cycle†	Citrate		0.86	0.85		
		Cis-aconitate		0.80	0.79		
		Succinate	0.68	0.65	0.96		
		Fumarate		0.87			
	Oxidative phosphorylation	Acetylphosphate	1.30				
		Pyrophosphate (PPi)*	1.67				

Table 1. Continued

Super Pathway	Sub Pathway	Biochemical Name	Fold Change			VIP Score	
			24 h vs. Ctrl	14 d vs. Ctrl	14 d vs. 24 h	14 d vs. Ctrl	14 d vs. 24 h
Lipid	Essential fatty acid	Docosahexaenoate (DHA; 22:6n3)*			0.72		1.89
	Medium-chain fatty acid	Caproate (6:0)*	0.80				
	Long-chain fatty acid	*Palmitoleate (16:1n7)*			*1.21*		2.03
	Fatty acid, ester	n-Butyl oleate*		1.65			
	Fatty acid metabolism (also BCAA metabolism)	Propionylcarnitine*		1.62			
	Carnitine metabolism	Carnitine*		1.24			
		3-dehydrocarnitine	0.71		1.35		
	Glycerolipid metabolism	Choline phosphate		1.37	1.45	2.05	2.07
		Glycerol 3-phosphate (G3P)		1.63	1.73	2.08	2.12
	Inositol metabolism	Myo-inositol			1.52		
	Sphingolipid	Sphinganine (safingol)	5.69	2.5†			
	Sterol/Steroid	Campesterol		2.14	1.48*	2.22	2.09
	Lysolipid†	2-arachidonoylglycerophosphoethanolamine	3.56	3.37			
		2-docosahexaenoylglycerophosphoethanolamine	3.38	2.48			
		1-palmitoylglycerophosphocholine	4.28	2.38	0.56		
		2-palmitoylglycerophosphocholine	2.99	2.64			
		1-stearoylglycerophosphocholine	4.73	3.34			
		1-oleoylglycerophosphocholine	3.23		0.53		
		2-oleoylglycerophosphocholine	3.97	2.20	0.55		
		2-arachidonoylglycerophosphocholine	5.05	3.02			
		2-docosahexaenoylglycerophosphocholine	3.70		0.33		
	Endocannabinoid†	Oleic ethanolamide	3.32		0.25		
		Palmitoyl ethanolamide	4.04	0.68	0.17		
		Stearoyl ethanolamide	9.82		0.10		
Nucleotides	Purine metabolism, adenine containing	Adenine			1.29		1.97
		Adenosine		0.66		2.08	
		N1-methyladenosine		*0.87*			1.94
	Purine metabolism, urate metabolism	Allantoin	2.06		0.52		2.00
	Pyrimidine metabolism, cytidine containing	Cytidine		1.29		2.09	
		2′-deoxycytidine			0.80		2.02
		5-methyl-2′-deoxycytidine	1.54		0.71		2.05
	Pyrimidine metabolism, uracil containing	Pseudouridine			0.79		1.94
	Purine and pyrimidine metabolism	Methylphosphate*		0.70		2.01	
Cofactors vitamins	Ascorbate and aldarate metabolism	Ascorbate (vitamin C)		1.50		2.03	
	Pantothenate and CoA metabolism	Pantothenate			1.62		2.06
		Phosphopantetheine			*1.47*		2.0
	Tocopherol metabolism	Alpha-tocopherol			1.37		1.95
Xenobiotics	Benzoate metabolism	Hippurate			0.59		
	Food component/plant	Ergothioneine		1.87	1.37	2.21	1.99
		Benzyl alcohol			*1.34*	1.91	
	Sugar, sugar substitute, starch	Erythritol		1.54	1.65	2.27	2.25

In the two right-most columns is shown the VIP score of biomarker metabolites for the two classes: 14 days versus control and 24 hours versus 14 days. In italics are shown those VIP metabolites whose regulation did not reach statistical significance.

Control values have been considered 1, hence values below 1 show downregulation and above 1 upregulation. Statistical significance (*P* value) for most of the metabolites was less than 0.1. Some metabolites reached statistical significance between 0.5 and 0.1 (*). Daggers (†) point to those metabolites whose statistics was influenced by outliers.

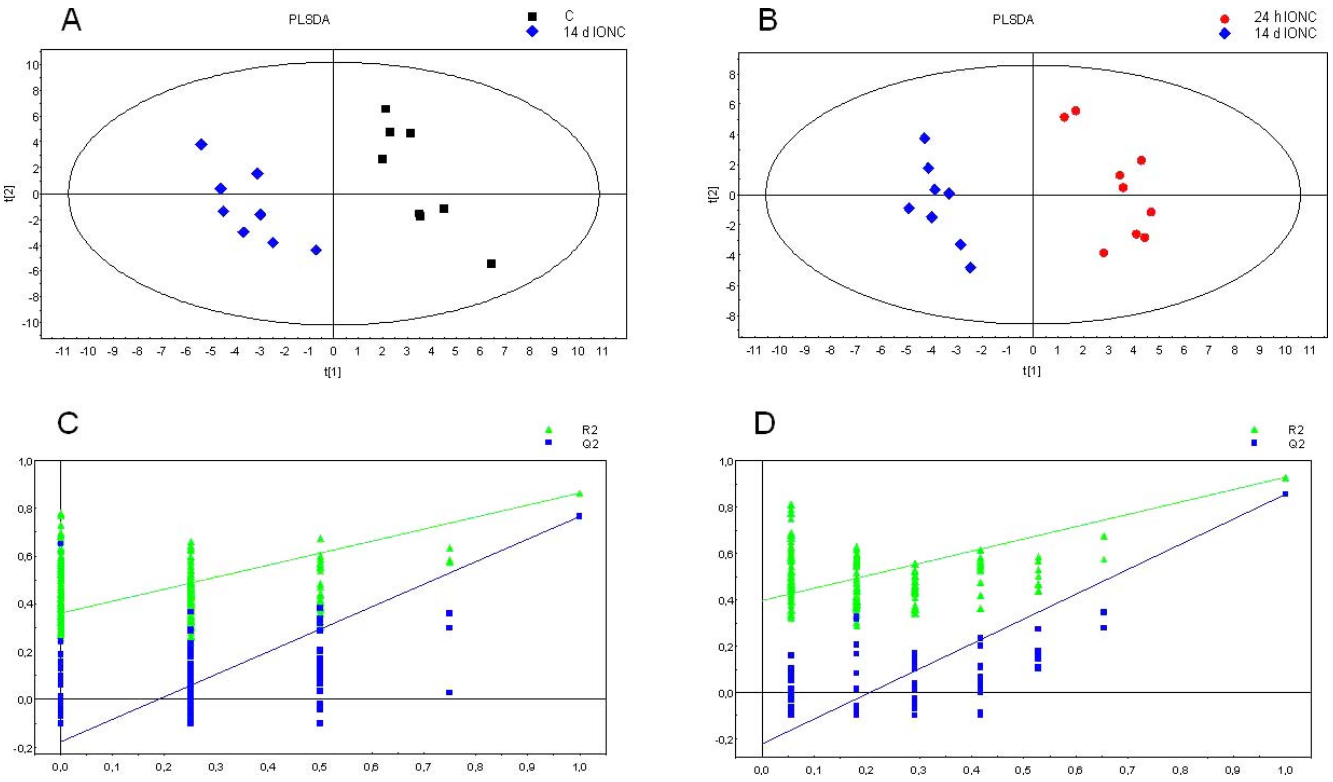

Figure 1. Retinal metabolome PLSDA score plots and model validation plots. PLSDA score plots (**A**, **B**) were obtained from comparing control versus 14 days post-IONC (**A**) and 24 hours post-IONC versus 14 days post-IONC (**B**). Model validation was obtained from 250 permutations test for the same comparisons ([**C**] and [**D**], respectively). The vertical axis shows the R^2 (goodness of the fit) and the Q^2 (goodness of the prediction). The horizontal axis represents the correlation between the "real" and the "permuted" *y*.

are directly related to dissimilarities between their metabolic profiles.

VIP score of each feature was obtained and used for potential biomarker selection using the "greater than one" rule.[47] Thus a total of 27 metabolites were selected to discriminate between control and 14-day injured retinas and 36 metabolites to discriminate between 24 hours and 14 days post-lesion (i.e., between early and late stages of degeneration). These metabolites were selected as potential biomarkers of neuronal degeneration (Table 1, two rightmost columns).

Functional Clustering

Enrichment analysis was performed for all the regulated metabolites and for the VIP metabolites separately to group them into the main signaling pathways or metabolic networks in which they participated. Only those maps or networks that had statistically significant changes in at least one of the comparisons were considered**.** The first observation was that both VIPs and regulated metabolites were clustered under the same processes, thus for the enrichment analyses in Table 2 and Supplementary Table S1, all metabolites were considered.

Clustering was obtained, mainly, with data from 14 days post-IONC. The metabolic networks (Supplementary Table S1) or pathway maps (Table 2) with a lower *P* value specifically regulated at this time point, either compared with control or with 24 hours were the following: arginine, asparagine and aspartic acid metabolism, (L)-arginine metabolism, fructose metabolism, glycolysis, glucogenesis and glucose transport, L-ornithine pathways, taurine and hypotaurine metabolism, galactose metabolism, urea cycle, pentose phosphate, and insulin regulation of glycogen metabolism. Metabolites with significant changes only in the 24 hours post-IONC group belonged to (L)-proline metabolism and phosphatidylcholine pathway.

Common to both time points were the tricarboxylic acid (TCA) cycle, alanine, glycine, cysteine and threonine metabolism, glycosphingolipid metabolism, N-acylethanolamines pathway, and glutathione metabolism.

Signaling map enrichment showed that canonical signaling cascades or biochemical pathways, such as oxidative stress, aminoacyl-t-RNA biosynthesis, sphingolipid metabolism, apoptosis through ceramide signaling, and glycolysis were regulated (Table 2).

Discussion

Here we describe the metabolomic changes occurring in the retina after IONC at two time points: before RGC loss is quantifiable (24 hours) and when the first quick wave of RGC death has ended (14 days[5,6]). The 24-hour time point analysis shows the metabolomic signature associated with RGCs committed to death but still alive (i.e., within the window frame) wherein neuroprotective therapies may be effective. The 14-day analysis shows the state of the stabilized retina after the injury, providing a pattern that may be useful to ameliorate the secondary degeneration associated with central nervous system insults, and to find possible biomarkers linked to neuronal degeneration.

Our analysis was carried out on whole-retinal extracts and thus it is not possible to ascribe the observed metabolomic changes to a specific retinal cell type. Although the observed regulation is triggered by the injury to RGCs, these changes are probably due to the activation of the retinal glia, astrocytes, Müller cells, and microglial cells, in response to RGC death.

Investigative Ophthalmology & Visual Science

Table 2. Signaling Pathway Maps Enrichment of the Metabolites Regulated in the Retina after IONC

Signaling Pathway Maps	*P* Value			No. of Regulated Metabolites	Total in Map
	IONC 24 h	IONC 14 d	IONC 24 h/14 d		
N-Acylethanolamines, N-Acyltransferase pathway	2.21E-05	7.02E-03	2.13E-04	3	32
N-Acylethanolamines, phospholipase A2 pathway	3.10E-05	8.71E-03	2.97E-04	4	40
Oxidative stress_role of ASK1 under oxidative stress	1.43E-03	7.02E-03	6.16E-03	2	34
Glutathione metabolism/rodent version	1.51E-03	6.13E-03	2.26E-03	4	71
Methionine-cysteine-glutamate metabolism	2.29E-03	5.25E-04	9.72E-03	3	43
TCA	3.21E-03	3.51E-05	1.35E-02	4	51
Aminoacyl-tRNA biosynthesis in cytoplasm/rodent version	4.64E-02	1.34E-03	1.86E-02	6	98
Glycine, serine, cysteine, and threonine metabolism/ rodent version	5.84E-02	3.20E-02	2.89E-02	4	125
Histidine-glutamate-glutamine metabolism	1.10E-02	4.95E-02		4	95
Sphingolipid metabolism	2.75E-02			2	91
Glycolysis and gluconeogenesis		3.00E-06	1.22E-04	4	66
Apoptosis and survival_ceramides signaling pathway	5.09E-02			2	40
Fructose metabolism/rodent version		3.36E-05	7.29E-04	4	84
Regulation of lipid metabolism_insulin regulation of glycogen metabolism		2.60E-04	6.37E-03	4	64
Galactose metabolism/rodent version		4.83E-04	4.09E-04	4	64
Urea cycle		5.04E-04	9.81E-03	5	70
(L)-Arginine metabolism		6.41E-04	1.15E-02	5	76
Regulation of lipid metabolism_insulin regulation of fatty acid metabolism		1.02E-03	1.55E-02	5	89
Taurine and hypotaurine metabolism		1.11E-03	4.67E-02	3	22
cAMP/Ca(2+)-dependent insulin secretion		2.21E-03	1.99E-03	2	43
(L)-Alanine, (L)-cysteine, and (L)-methionine metabolism		7.09E-03	6.37E-03	3	56
Polyamine metabolism		1.15E-02	1.04E-02	3	68
Selenoamino acid metabolism		1.71E-02	1.51E-02	3	54
Beta-alanine metabolism/rodent version		2.36E-03		2	32
Aspartate and asparagine metabolism		1.18E-02		3	73

"Regulated metabolites" refers to the total number of metabolites regulated by IONC that belong to a given map. "Total in maps" means the total number of metabolites that belong to that map. *P* value means the probability of a random intersection of two different gene sets. h, hours postlesion; d, days postlesion. This analysis was carried out using the Metacore platform.

The upregulation of sphinganine, however, is probably caused by RGCs themselves, as this compound is linked to the ceramide apoptotic pathway, a signaling route highly regulated by axotomy in these neurons (see below).

Although a large number of metabolites was analyzed, not all metabolites present in the retina were identified, as this was a targeted analysis focused on 195 metabolites. Thus, there will probably be metabolomic changes not detected and pathways not analyzed, particularly metabolites present in a low concentration or with lipophilic physical characteristics.

A PLSDA analysis of all detected metabolites was performed, allowing us to select which metabolites were significantly altered after the injury. This analysis showed that there was a clear separation between 24 hours versus 14 days post-IONC groups. These findings are in agreement with previous reports in the literature showing that during the first 2 days after the injury,[5–9] while there is an upregulation of cellular signals leading to cell death, there is not a significant RGC loss, and, thus, there were few specifically regulated metabolites. In particular, VIP metabolites identified at 14 days could act as diagnostic markers of retinal degeneration or as future therapeutic targets such as urea, sorbitol, glucose, or fructose.

Among these, our analysis shows that sphinganine (safingol), a ceramide precursor, while not detected in all samples, was more than 5.0- and 2.5-fold higher at 24 hours and 14 days post-IONC, respectively, than in control, indicating a rapid accumulation of sphinganine after IONC and a posterior decrease, although still higher than control levels. At 14 days post-IONC, an increase of choline-phosphate, a product of the sphingomyelin degradation that ends producing ceramide, was also detected. Our metabolic analysis did not detect ceramide due to its lypophilic nature. Ceramide molecules regulate diverse signaling pathways involving apoptosis, cell senescence, cell cycle, and differentiation.[48] In general, ceramide effects are antagonistic to growth and survival.

As depicted in Figure 2A, safingol upregulation might reflect an activation of the apoptotic ceramide signaling pathway. This pathway commences at the tumor necrosis factor receptor 1 (TNFR1), a receptor that has been reported to be overexpressed by RGCs after IONC[8] and in glaucomatous degeneration.[49] TNFR1 signals through *FADD* and *TRADD*, both of which are upregulated by RGCs after IONC.[9,50] This leads to the activation of caspase 8, which in turn activates caspase 3. Interestingly, both caspases are as well overexpressed by RGCs after IONC.[8,51] Taken together, these results indicate that IONC induces a protein and metabolic activation of the apoptotic ceramide signaling pathway, which also inhibits glucose uptake,[52] a change also detected in this work (Fig. 2B, see below).

At 24 hours and 14 days, an inverse regulation of N-acylethanolamines (NAEs) was observed. NAEs are endogenous lipids that are synthesized and accumulated in response to tissue injury.[53] They are believed to be neuroprotectants that reduce apoptosis and inflammation.[54] NAEs are part of the endocannabinoid metabolism. Endocannabinoids are constitutively expressed in the retina, and it has been reported that

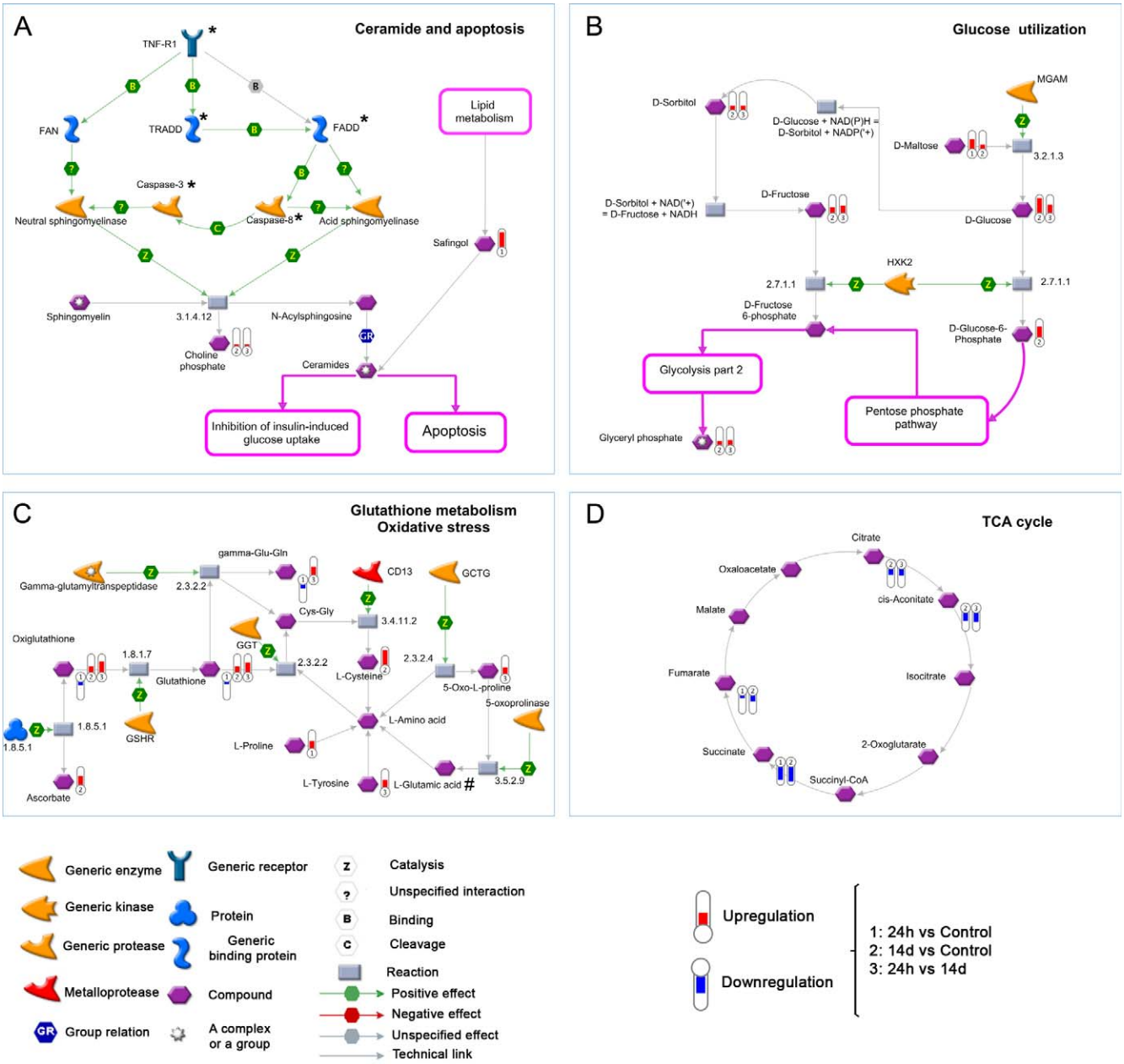

Figure 2. Signaling maps based on the metabolite regulation in the retina by IONC. (**A**) Extrinsic apoptotic pathway mediated by ceramides. *TNFR1, FADD, TRADD, Caspase 3, and Caspase 8 proteins are overexpressed in the RGCs after IONC[895,051]. (**B**) Glucose utilization. (**C**) Glutathione metabolism and oxidative stress. L-glutamic acid (glutamate) was not significantly regulated but was nevertheless included in the map because it scored as a VIP metabolite. (**D**) Tricarboxylic acid cycle. Interactions and enzymatic reactions are described in Supplementary Table S2. Maps were created using the Pathway Map Creator tool from Metacore.

their downregulation in a model of glaucoma may play a role in glaucoma-associated RGC death.[55] Thus, the upregulation of these lipids at 24 hours after IONC may reflect an early activation of protective signals of the retina.

On the other hand, the PLSDA analysis of the 14 days post-IONC samples, when the proapoptotic signals had decreased and the RGC loss was depleted to 85% of the original population, showed that the number of altered metabolites was substantially increased. At this time point, the metabolism of amino acids was deregulated, provoking the accumulation of putrescine, a product of the amino acid catabolism. Although putrescine has also been shown to act as neuroprotectant,[56] its increase at 14 dpl would probably be a reflection of amino acid catabolism rather than a protective signal, since at 14 dpl most of the RGCs have already died. Furthermore, at this time point, the aminoacyl t-RNA biosynthesis pathway was downregulated, which indicates an alteration of translation and suggest that protein synthesis in the injured retinas is below normal levels, as it has been reported in glaucoma and ischemia.[57,58]

One of the most consistent differences observed at 14 days post-IONC was associated with carbohydrate metabolism. Glucose (Glc) and glucose-6-phospate (Glc-6-P) levels were nearly 3-fold higher 14 days post-IONC, whereas additional glycolytic intermediates (3-phosphoglycerate, 2-phospoglycer-

ate, and lactate) were slightly higher, but not significantly different from the control (Table 1, Fig. 2B). To alleviate the high glucose levels and prevent retinal damage, glucose was diverted into the sorbitol pathway, resulting in sorbitol and fructose accumulation (both significantly higher at 14 days post-IONC). There was also an increase of glyceryl phosphate, an intermediate during the second part of the glycolysis pathway. These results suggest that IONC induces a deregulation of the carbohydrate metabolism that may result in a compromised cellular energy status, since the TCA cycle is also altered (see below, Fig. 2D). Finally, our analysis marked fructose, glucose, and glucose-6-phosphate as VIP metabolites and thus may be used as biomarkers of the late steps of neuronal degeneration.

Hypotaurine and urea were higher in the injured retina after 14 days compared with the control retinas. Urea, as sorbitol, glucose, myo-inositol, betaine, and erythritol, is an osmolyte.[59] All of them were higher in the 14 days post-IONC, indicating an increase in osmotic stress in the injured retina.

In the diabetic retina, hyperglycemia leads to an increase in the cell oxidative stress status.[60] Oxidative stress also occurs in glaucomatous retinas, and antioxidant therapies have been shown to be neuroprotective in this pathology.[61] In this study, glutathione (oxidized and reduced) was downregulated at 24 hours post-IONC, but together with vitamin C (ascorbic acid) was slightly higher in 14 days post-IONC rats as compared with controls (Fig. 2C). The detected high levels of cysteine-glutathione disulfide, which is formed from glutathione during oxidative stress, may be an indicator of increased oxidative stress.[62] In addition to this, ascorbate and ergothioneine (a powerful scavenger of hydroxyl radicals and an inhibitor of iron or copper ion-dependent generation of hydroxyl radicals from H_2O_2) were significantly higher 14 days post-IONC and may act as a compensatory mechanism to deal with the increase in oxidative stress following injury.

Consistent with limited glycolysis in the retina, lower levels of TCA intermediates (citrate, cis-aconitate, succinate, fumarate, and malate) were detected at both times post-IONC (Fig. 2D). Although these differences were partially skewed by outliers, they suggest a lower level of metabolite flux through the TCA cycle, indicating an overall difference in mitochondrial function, which could contribute to differences in oxidative stress between the control and post-IONC rat.

In conclusion, we have described the metabolomic alterations induced in the rat retina after axonal crush, showing clear differences between the early and late stages of degeneration. The identification of potential biomarkers paves the road for further analysis and validation in human samples. Analysis of concentration changes of these discriminating metabolites in human retinas may help identify prognostic factors or therapeutic target molecules during retinal or neuronal degeneration.

Acknowledgments

Supported by the Spanish Ministry of Economy and Competitiveness (BFU2009-10808), Instituto de Salud Carlos III Fondo Europeo de Desarrollo Regional "Una manera de hacer Europa" (PI10/00187, PI11/02942), Conselleria de Educación Generalitat Valenciana (ACOMP2011/136), Fundación Séneca (04446/GERM/07), Spanish Ministry of Education and Science (SAF-22010-10385), and Red Temática de Investigación Cooperativa en Oftalmología (RD07/0062/0001).

Disclosure: **M. Agudo-Barriuso**, None; **A. Lahoz**, None; **F.M. Nadal-Nicolás**, None; **P. Sobrado-Calvo**, None; **M. Piquer-Gil**, None; **M. Díaz-Llopis**, None; **M. Vidal-Sanz**, None; **J.L. Mullor**, None

References

1. Resnikoff S, Pascolini D, Etya'ale D, et al. Global data on visual impairment in the year 2002. *Bull World Health Organ*. 2004;82:844–851.
2. Agudo-Barriuso M, Villegas-Perez M, de Imperial JM, Vidal-Sanz M. Anatomical and functional damage in experimental glaucoma. *Curr Opin Pharmacol*. 2013;13:5–11.
3. Vidal-Sanz M, Salinas-Navarro M, Nadal-Nicolas FM, et al. Understanding glaucomatous damage: anatomical and functional data from ocular hypertensive rodent retinas. *Prog Retin Eye Res*. 2012;31:1–27.
4. Almasieh M, Wilson AM, Morquette B, Cueva Vargas JL, DiPolo A. The molecular basis of retinal ganglion cell death in glaucoma. *Prog Retin Eye Res*. 2012;31:152–181.
5. Parrilla-Reverter G, Agudo M, Sobrado-Calvo P, Salinas-Navarro M, Villegas-Perez MP, Vidal-Sanz M. Effects of different neurotrophic factors on the survival of retinal ganglion cells after a complete intraorbital nerve crush injury: a quantitative in vivo study. *Exp Eye Res*. 2009;89:32–41.
6. Nadal-Nicolas FM, Jimenez-Lopez M, Sobrado-Calvo P, et al. Brn3a as a marker of retinal ganglion cells: qualitative and quantitative time course studies in naive and optic nerve-injured retinas. *Invest Ophthalmol Vis Sci*. 2009;50:3860–3868.
7. Nadal-Nicolás FM, Jiménez-López M, Salinas-Navarro M, et al. Whole number, distribution and co-expression of brn3 transcription factors in retinal ganglion cells of adult albino and pigmented rats. *PLoS One*. 2012;7:e49830.
8. Agudo M, Perez-Marin MC, Lonngren U, et al. Time course profiling of the retinal transcriptome after optic nerve transection and optic nerve crush. *Mol Vis*. 2008;14:1050–1063.
9. Agudo M, Perez-Marin MC, Sobrado-Calvo P, et al. Immediate upregulation of proteins belonging to different branches of the apoptotic cascade in the retina after optic nerve transection and optic nerve crush. *Invest Ophthalmol Vis Sci*. 2009;50:424–431.
10. Cheng L, Sapieha P, Kittlerova P, Hauswirth WW, Di PA. TrkB gene transfer protects retinal ganglion cells from axotomy-induced death in vivo. *J Neurosci*. 2002;22:3977–3986.
11. Leaver SG, Cui Q, Plant GW, et al. AAV-mediated expression of CNTF promotes long-term survival and regeneration of adult rat retinal ganglion cells. *Gene Ther*. 2006;13:1328–1341.
12. Lebrun-Julien F, DiPolo A. Molecular and cell-based approaches for neuroprotection in glaucoma. *Optom Vis Sci*. 2008;85:417–424.
13. Mansour-Robaey S, Clarke DB, Wang YC, Bray GM, Aguayo AJ. Effects of ocular injury and administration of brain-derived neurotrophic factor on survival and regrowth of axotomized retinal ganglion cells. *Proc Natl Acad Sci U S A*. 1994;91:1632–1636.
14. Peinado-Ramon P, Salvador M, Villegas-Perez MP, Vidal-Sanz M. Effects of axotomy and intraocular administration of NT-4, NT-3, and brain-derived neurotrophic factor on the survival of adult rat retinal ganglion cells. A quantitative in vivo study. *Invest Ophthalmol Vis Sci*. 1996;37:489–500.
15. Sanchez-Migallon MC, Nadal-Nicolas FM, Jimenez-Lopez M, Sobrado-Calvo P, Vidal-Sanz M, Agudo-Barriuso M. Brain derived neurotrophic factor maintains Brn3a expression in axotomized rat retinal ganglion cells. *Exp Eye Res*. 2011;92:260–267.
16. Saragovi HU, Hamel E, Di PA. A neurotrophic rationale for the therapy of neurodegenerative disorders. *Curr Alzheimer Res*. 2009;6:419–423.
17. Weibel D, Kreutzberg GW, Schwab ME. Brain-derived neurotrophic factor (BDNF) prevents lesion-induced axonal die-back in young rat optic nerve. *Brain Res*. 1995;679:249–254.

18. Nicholson JK, Holmes E, Elliott P. The metabolome-wide association study: a new look at human disease risk factors. *J Proteome Res*. 2008;7:3637–3638.
19. Monteiro MS, Carvalho M, Bastos MD, de Pinho PG. Metabolomics analysis for biomarker discovery: advances and challenges. *Curr Med Chem*. 2013;20:257–271.
20. Weiner J III, Parida SK, Maertzdorf J, et al. Biomarkers of inflammation, immunosuppression and stress with active disease are revealed by metabolomic profiling of tuberculosis patients. *PLoS One*. 2012;7:e40221.
21. Suh JH, Kim RY, Lee DS. A new metabolomic assay to examine inflammation and redox pathways following LPS challenge. *J Inflamm (Lond)*. 2012;9:37.
22. Ganti S, Taylor SL, Abu AO, et al. Kidney tumor biomarkers revealed by simultaneous multiple matrix metabolomics analysis. *Cancer Res*. 2012;72:3471–3479.
23. Denkert C, Bucher E, Hilvo M, et al. Metabolomics of human breast cancer: new approaches for tumor typing and biomarker discovery. *Genome Med*. 2012;4:37.
24. O'Connell TM. Recent advances in metabolomics in oncology. *Bioanalysis*. 2012;4:431–451.
25. Kim OY, Lee JH, Sweeney G. Metabolomic profiling as a useful tool for diagnosis and treatment of chronic disease: focus on obesity, diabetes and cardiovascular diseases. *Expert Rev Cardiovasc Ther*. 2013;11:61–68.
26. Langley SR, Dwyer J, Drozdov I, Yin X, Mayr M. Proteomics: from single molecules to biological pathways. *Cardiovasc Res*. 2013;97:612–622.
27. Turer AT. Using metabolomics to assess myocardial metabolism and energetics in heart failure. *J Mol Cell Cardiol*. 2013; 55:12–18.
28. Senn T, Hazen SL, Tang WH. Translating metabolomics to cardiovascular biomarkers. *Prog Cardiovasc Dis*. 2012;55:70–76.
29. Webhofer C, Gormanns P, Reckow S, et al. Proteomic and metabolomic profiling reveals time-dependent changes in hippocampal metabolism upon paroxetine treatment and biomarker candidates. *J Psychiatr Res*. 2013;47:289–298.
30. Han X, Rozen S, Boyle SH, et al. Metabolomics in early Alzheimer's disease: identification of altered plasma sphingolipidome using shotgun lipidomics. *PLoS One*. 2011;6: e21643.
31. Sato Y, Suzuki I, Nakamura T, Bernier F, Aoshima K, Oda Y. Identification of a new plasma biomarker of Alzheimer's disease using metabolomics technology. *J Lipid Res*. 2012;53: 567–576.
32. Trushina E, Nemutlu E, Zhang S, et al. Defects in mitochondrial dynamics and metabolomic signatures of evolving energetic stress in mouse models of familial Alzheimer's disease. *PLoS One*. 2012;7:e32737.
33. Bazenet C, Lovestone S. Plasma biomarkers for Alzheimer's disease: much needed but tough to find. *Biomark Med*. 2012; 6:441–454.
34. Hassan-Smith G, Wallace GR, Douglas MR, Sinclair AJ. The role of metabolomics in neurological disease. *J Neuroimmunol*. 2012;248:48–52.
35. Ma Y, Zhang P, Wang F, Liu W, Yang J, Qin H. An integrated proteomics and metabolomics approach for defining oncofetal biomarkers in the colorectal cancer. *Ann Surg*. 2012;255:720–730.
36. Blanchet L, Smolinska A, Attali A, et al. Fusion of metabolomics and proteomics data for biomarkers discovery: case study on the experimental autoimmune encephalomyelitis. *BMC Bioinformatics*. 2011;12:254.
37. Cavill R, Kamburov A, Ellis JK, et al. Consensus-phenotype integration of transcriptomic and metabolomic data implies a role for metabolism in the chemosensitivity of tumour cells. *PLoS Comput Biol*. 2011;7:e1001113.
38. Eckel-Mahan KL, Patel VR, Mohney RP, Vignola KS, Baldi P, Sassone-Corsi P. Coordination of the transcriptome and metabolome by the circadian clock. *Proc Natl Acad Sci U S A*. 2012;109:5541–5546.
39. Fabisiak JP, Medvedovic M, Alexander DC, et al. Integrative metabolome and transcriptome profiling reveals discordant energetic stress between mouse strains with differential sensitivity to acrolein-induced acute lung injury. *Mol Nutr Food Res*. 2011;55:1423–1434.
40. Perco P, Muhlberger I, Mayer G, Oberbauer R, Lukas A, Mayer B. Linking transcriptomic and proteomic data on the level of protein interaction networks. *Electrophoresis*. 2010;31:1780–1789.
41. Xie Z, Li H, Wang K, et al. Analysis of transcriptome and metabolome profiles alterations in fatty liver induced by high-fat diet in rat. *Metabolism*. 2010;59:554–560.
42. Zhang Y, Filiou MD, Reckow S, et al. Proteomic and metabolomic profiling of a trait anxiety mouse model implicate affected pathways. *Mol Cell Proteomics*. 2011;10: M111.
43. Zhang Y, Zhang X, Wu B, Cheng S. Evaluating the transcriptomic and metabolic profile of mice exposed to source drinking water. *Environ Sci Technol*. 2012;46:78–83.
44. Parrilla-Reverter G, Agudo M, Nadal-Nicolas F, et al. Time-course of the retinal nerve fibre layer degeneration after complete intra-orbital optic nerve transection or crush: a comparative study. *Vision Res*. 2009;49:2808–2825.
45. Quintas G, Garcia-Cañaveras JC, Castell JV, Ferrer A, Lahoz A. Chemometric approaches to improve PLSDA model outcome for predicting human non-alcoholic fatty liver disease using UPLC-MS as a metabolic profiling tool. *Metabolomics*. 2012;8: 86–98.
46. Lindgren F, Hansen B, Karcher W, Sjöström M, Eriksson M. Model validation by permutation tests: Applications to variable selection. *J Chemom*. 1996;10:521–532.
47. Chong IG, Jun CH. Performance of some variable selection methods when multicollinearity is present. *Chemom Intell Lab Syst*. 2005;78:103–112.
48. Mathias S, Pena LA, Kolesnick RN. Signal transduction of stress via ceramide. *Biochem J*. 1998;335:465–480.
49. Tezel G. TNF-alpha signaling in glaucomatous neurodegeneration. *Prog Brain Res*. 2008;173:409–421.
50. Agudo M, Nadal-Nicolas FM, Perez-Marin MC, et al. TNFR1 death-signalling pathway is regulated in the retina after optic nerve transection and optic nerve crush. *Invest Ophthalmol Vis Sci*. 2009;50:3467.
51. Weishaupt JH, Diem R, Kermer P, Krajewski S, Reed JC, Bahr M. Contribution of caspase-8 to apoptosis of axotomized rat retinal ganglion cells in vivo. *Neurobiol Dis*. 2003;13:124–135.
52. Stratford S, Hoehn KL, Liu F, Summers SA. Regulation of insulin action by ceramide: dual mechanisms linking ceramide accumulation to the inhibition of Akt/protein kinase B. *J Biol Chem*. 2004;279:36608–36615.
53. Hansen HH, Ikonomidou C, Bittigau P, Hansen SH, Hansen HS. Accumulation of the anandamide precursor and other N-acylethanolamine phospholipids in infant rat models of in vivo necrotic and apoptotic neuronal death. *J Neurochem*. 2001; 76:39–46.
54. Garg P, Duncan RS, Kaja S, Koulen P. Intracellular mechanisms of N-acylethanolamine-mediated neuroprotection in a rat model of stroke. *Neuroscience*. 2010;166:252–262.
55. Nucci C, Bari M, Spano A, et al. Potential roles of (endo)cannabinoids in the treatment of glaucoma: from intraocular pressure control to neuroprotection. *Prog Brain Res*. 2008;173:451–464.

Investigative Ophthalmology & Visual Science

56. Harada J, Sugimoto M. Polyamines prevent apoptotic cell death in cultured cerebellar granule neurons. *Brain Res*. 1997;753: 251–259.
57. Bakalash S, Pham M, Koronyo Y, et al. Egr1 expression is induced following glatiramer acetate immunotherapy in rodent models of glaucoma and Alzheimer's disease. *Invest Ophthalmol Vis Sci*. 2011;52:9033–9046.
58. Kamphuis W, Dijk F, van Soest S, Bergen AA. Global gene expression profiling of ischemic preconditioning in the rat retina. *Mol Vis*. 2007;13:1020–1030.
59. Brocker C, Thompson DC, Vasiliou V. The role of hyperosmotic stress in inflammation and disease. *Biomol Concepts*. 2012;3:345–364.
60. Hernandez C, Simo R. Neuroprotection in diabetic retinopathy. *Curr Diab Rep*. 2012;12:329–337.
61. Chidlow G, Wood JP, Casson RJ. Pharmacological neuroprotection for glaucoma. *Drugs*. 2007;67:725–759.
62. Lu SC. Glutathione synthesis. *Biochim Biophys Acta*. 2013; 1830:3143–3153.

Investigative Ophthalmology & Visual Science